Journal of
Mechanics of
Materials and Structures

Xin Qu, Fangfang Diao, Xingqian Xu and Wei Li

msp

msp

BENDING OF NONCONFORMING THIN PLATES BASED ON THE FIRST-ORDER MANIFOLD METHOD

XIN QU, FANGFANG DIAO, XINGQIAN XU AND WEI LI

As the convergence, good numerical accuracy and high computing efficiency of nonconforming elements cannot be achieved simultaneously using the finite element method (FEM) or the current numerical manifold method (NMM), the first-order NMM was developed to analyze the bending of thin plates. The first-order Taylor expansion was selected to construct the local displacement function, which endowed the generalized degrees of freedom with physical meanings and decreased the rank deficiency. Additionally, the new relations between the global and local rotation functions in the first-order approximation were derived by adopting two sets of rotation functions, $\{\theta_{xi}, \theta_{yi}\}$ and $\{\theta_x{}^i, \theta_y{}^i\}$. Regular meshes were selected to improve the convergence performance. With the penalized formulation fitted to the NMM for Kirchhoff's thin plate problems, a unified scheme was proposed to deal with irregular and regular boundaries of the domain. The typical examples indicated that the numerical solutions achieved using the first-order NMM rapidly converged to the analytical solutions, and the accuracy of such numerical solutions was vastly superior to that achieved using the FEM and the zero-order NMM.

1. Introduction

A thin plate is one of the most widely used essential structural components, and the numerical analysis of such thin plate with the finite element method (FEM) has provided important guidance for applications in structural engineering [Deng and Murakawa 2008; Kersemans et al. 2014; Miyazaki et al. 2016; Xing and Liu 2009]. The bending of thin plates is associated with fourth-order differential equations, and the classical thin plate theory based on the assumptions formalized by Kirchhoff demands both the transverse displacement and normal rotation to be continuous, i.e., C^1 continuous [Ciarlet 1978; Timoshenko and Woinowsky-Krieger 1959]. This requirement makes it difficult to construct conforming elements. The solution obtained with conforming elements will give bounds to the energy of the correct solution, but, will yield inferior accuracy to that achieved with nonconforming elements on many occasions [Liu and Trung 2010; Zienkiewicz and Taylor 2005]. Thus, such nonconforming elements are often recommended for practical usage. Unfortunately, the convergence of these nonconforming elements significantly depends on the mesh regularity [Ciarlet 1978; Lascaux and Lesaint 1975; Shi 1984]. Furthermore, regular meshes cannot be available for FEM in some cases, particularly in a domain with irregular physical boundaries. Although the mesh-dependence phenomenon of nonconforming elements can be overcome using transformed elements [Shi 1990; Tang et al. 1981; Zhao 1988], the traditional method of constructing displacement functions is not fitted to these transformed elements and good numerical performance cannot be achieved with one element in any situation through numerical experience [Zheng et al. 2013]. Since two completely independent cover systems are used in the numerical manifold method (NMM),

regular meshes can always be selected to improve the convergence performance [Shi 1991], which can solve the abovementioned problems.

At present, some achievements have been made in the analysis of thin plate bending using the NMM. For instance, Zhou and Deng [2008], Zheng et al. [2013] and Qu et al. [2016] solved the convergence problem of nonconforming elements using variational principles, which demonstrated that the NMM provided an alternative way to rescue nonconforming elements. Zhang et al. [2010], Luo et al. [2010] and Wen and Luo [2012] proposed different methods to construct weighted functions, which successfully increased the computational accuracy and convergence rate. These achievements obtained using the NMM further developed the theory of thin plate bending problems. However, these studies still had some issues to be resolved. For the first three studies, the accuracy was not satisfactory when dealing with complex boundary conditions. For the other studies, considerable effort was required to construct shape functions and the applicability was not widespread, reducing the efficiency. Thus, it is necessary to establish a new method that takes into account the accuracy, efficiency, and convergence.

In this study, the first-order Taylor expansion was employed to construct the local displacement function, which endowed the generalized degrees of freedom with physical meanings [Qu and Zheng 2014] and decreased the rank deficiency [Xu et al. 2014]. Obviously, the first-order approximation is the most economical way to upgrade the order of the local deflection function. Additionally, the new relations between the global and local rotation functions in the first-order approximation were derived by adopting two sets of rotation functions, $\{\theta_{xi}, \theta_{yi}\}$ and $\{\theta_x{}^i, \theta_y{}^i\}$. Regular meshes were selected to improve the convergence performance since two completely independent cover systems were used in the NMM. In this way, the best interpolation accuracy, good convergence performance and high computational efficiency can be achieved in the analysis of thin plate bending using the first-order NMM. Then, with the penalized formulation fitted to the NMM for Kirchhoff's thin plate problems, a unified scheme was proposed to deal with irregular and regular boundaries of the domain, and the corresponding computational procedure is introduced in this paper. Finally, three numerical examples were presented to verify the first-order NMM by comparing with the results achieved using the FEM and the zero-order NMM.

2. First-order NMM

In general, the integration over the entire problem is divided into a summation of integrations over all the elements, and the solution is constructed by an interpolation polynomial. However, the continuity of the normal rotation on element surfaces in a nonconforming thin plate cannot be achieved. Thus, the continuous requirements for the variation of the interpolation function cannot be satisfied in this case, which leads to a linear δ-type singular distribution of some derivatives. Importantly, the legality of using the Green theorem cannot be guaranteed, and the final numerical solutions may not always converge to the analytical solutions. The "patch test" proposed in [Bazeley et al. 1965], is considered to be a standard approach for testing the convergence of nonconforming elements. If an element can pass the "patch test", its convergence can be achieved [Bazeley et al. 1965]. The existing literature [Wang 2003; Xie 2009; Zienkiewicz and Taylor 2005] and numerical experience have shown that the elements formed by regular meshes, as proposed by the NMM, are able to pass the "patch test". Therefore, in this paper, rectangular meshes were selected to analyze thin plate bending problems.
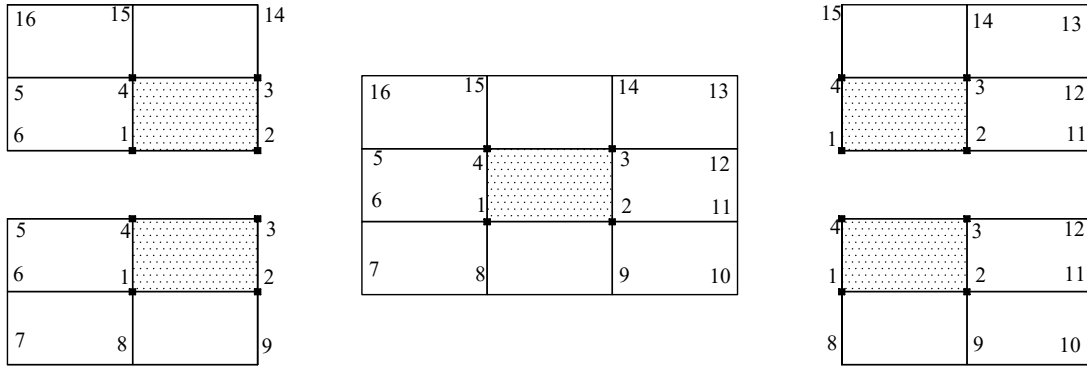
Figure 1. A manifold element and its "physical stars".

A series of the identical rectangular meshes called the finite element meshes were employed as mathematical meshes to cover the neutral surface of a thin plate. In the mathematical covers, one mathematical patch corresponding to one node was the domain composed of rectangular elements connected to it (customarily called a "mathematical star"). Taking Figure 1 as an example, mathematical star 1 is the large rectangle 7-8-9-2-3-4-5-6 that contains four small rectangles 7-8-1-6, 8-9-2-1, 1-2-3-4 and 6-1-4-5; mathematical star 2 is the large rectangle 8-9-10-11-12-3-4-1 that contains four small rectangles 8-9-2-1, 9-10-11-2, 2-11-12-3 and 1-2-3-4; mathematical star 3 is the large rectangle 1-2-11-12-13-14-15-4 that contains four small rectangles 1-2-3-4, 2-11-12-3, 3-12-13-14 and 4-3-14-15; mathematical star 4 is the large rectangle 6-1-2-3-14-15-16-5 that contains four small rectangles 6-1-4-5, 1-2-3-4 , 4-3-14-15 and 5-4-15-16.

By intersecting the neutral surface of the thin plate with all the mathematical stars, "physical stars" can be achieved. All the physical stars constitute physical covers or physical meshes. The overlapping domain of four physical stars forms a manifold element. In Figure 1, the mathematical meshes match the problem domain, and thus, the mathematical stars are the physical stars. The overlapping domain of the physical stars 1, 2, 3 and 4 is the rectangle 1-2-3-4, which is a manifold element.

By cohering four physical stars with their corresponding weighted (shape) functions, the global deflection function of a manifold element can be obtained as

$$w = \sum_{i=1}^{4} N_i \delta_i, \quad (i = 1, 2, 3, 4), \tag{1}$$

where N_i is the weighted (shape) function of physical star i, and δ_i is the local displacement function of physical star i.

2.1. First-order local displacement function.

In general, there are two ways to upgrade the order of the global displacement function, i.e., constructing a high-order shape function and adopting a high-order local displacement function. However, equation (9) is difficult to satisfy, and thus, constructing the high-order shape function is difficult in the bending of the nonconforming thin plate. Thus, constructing the high-order local displacement function becomes the only reasonable way to upgrade the order of the global displacement function. Lagrange and Hermite piecewise interpolation polynomials are often

used to construct the local displacement functions. Since the derivatives of the deflection function at nodes must be retained in the thin plate bending analysis, Hermite piecewise interpolation functions were adopted in this study.

Once the high-order local displacement function is adopted, more generalized degrees of freedom will be generated. However, the constraint equations do not increase correspondingly. Therefore, the constraint strength of an element is decreased, which may make the element convergence worse. Fortunately, this risk can be reduced to a minimum in the NMM, because the two completely independent cover systems allow the best meshes to be selected as the mathematical meshes for interpolation to improve the convergence performance, such as the rectangular meshes selected in the previous analysis.

In principle, it is available for each physical star to be assigned independently a local deflection function, $w_i(x, y)$, and a local rotation function about the x axis, $\theta_{xi}(x, y)$, and a local rotation function about the y axis, $\theta_{yi}(x, y)$. The undetermined constants in these three functions are uniformly characterized as the generalized degrees of freedom. When constants are chosen as the deflection and rotation functions, it renders the so-called zero-order approximation. For the zero-order approximation, if mathematical meshes match physical meshes, the results are almost the same as those achieved using the FEM. When a linear polynomial is selected as the local deflection function and constants are employed as the local rotation functions about the x and y axes, it is called the first-order approximation. Obviously, the first-order approximation is the most economical way to upgrade the order of the local deflection function. Thus, the first-order approximation was selected to construct a high-order local displacement function.

To endow the generalized degrees of freedom with physical meanings, the local deflection function was constructed following a previously reported method [Qu and Zheng 2014; Xu et al. 2014]. The local deflection function $w_i(x, y)$ was regarded as the first-order Taylor expansion of the global deflection function $w(x, y)$ at (x_i, y_i), which can be written as

$$w_i(x, y) = w^i + w_x^i(x - x_i) + w_y^i(y - y_i), \tag{2}$$

$$w^i = w(x_i, y_i), \quad w_x^i = \left.\frac{\partial w(x, y)}{\partial x}\right|_{(x_i, y_i)}, \quad w_y^i = \left.\frac{\partial w(x, y)}{\partial y}\right|_{(x_i, y_i)}. \tag{3}$$

The physical relations between the global deflection and rotation functions can be expressed as

$$-\theta_y = \frac{\partial w(x, y)}{\partial x}, \quad \theta_x = \frac{\partial w(x, y)}{\partial y}, \tag{4}$$

where θ_x and θ_y denote the global rotation functions about the x and y axes, respectively.

Then, (2) can be also written as

$$w_i(x, y) = w^i - \theta_y^i(x - x_i) + \theta_x^i(y - y_i), \tag{5}$$

where θ_x^i and θ_y^i, induced by the local deflection function $w_i(x, y)$ at (x_i, y_i), are called the additional rotation functions.

Therefore, the local displacement function can be written as

$$
\left\{ \begin{array}{c} w_i(x,\,y) \\ \theta_{xi} \\ \theta_{yi} \end{array} \right\} = \begin{pmatrix} 1 & 0 & 0 & -(x-x_i) & y-y_i \\ 0 & 1 & 0 & 0 & 0 \\ 0 & 0 & 1 & 0 & 0 \end{pmatrix} \left\{ \begin{array}{c} w^i \\ \theta_{xi} \\ \theta_{yi} \\ \theta_y^i \\ \theta_x^i \end{array} \right\},
\tag{6}
$$

where θ_{xi} and θ_{yi} denote the local rotation functions about the x and y axes, respectively.

From (6), the generalized degrees of freedom array of physical star i in the first-order approximation can be written as

$$
\{\delta_i\} = \left\{ \begin{array}{c} \{w_i\} \\ \theta_{xi} \\ \theta_{yi} \end{array} \right\} = \left\{ \begin{array}{c} w^i \\ \theta_{xi} \\ \theta_{yi} \\ \theta_y^i \\ \theta_x^i \end{array} \right\}.
\tag{7}
$$

Since every manifold element is formed by four overlapping physical stars, there are 20 degrees of freedom in a manifold element. Substituting (7) into (1), the global deflection function of an element can be given as

$$
w = \sum_{i=1}^{4} N_i\,\delta_i = \sum_{i=1}^{4} N_i\,w^i + N_{xi}\,\theta_{xi} + N_{yi}\,\theta_{yi} + N_i\,\theta_x^i(y-y_i) - N_i\,\theta_y^i(x-x_i),
\tag{8}
$$

where $N_i = [N_i,\,N_{xi},\,N_{yi}]$ must meet (9):

$$
\begin{aligned}
N_i(r_j) &= \delta_{ij}, & \frac{\partial N_i(r_j)}{\partial x} &= 0, & \frac{\partial N_i(r_j)}{\partial y} &= 0, \\
N_{xi}(r_j) &= 0, & \frac{\partial N_{xi}(r_j)}{\partial x} &= 0, & \frac{\partial N_{xi}(r_j)}{\partial y} &= \delta_{ij}, \\
N_{yi}(r_j) &= 0, & \frac{\partial N_{yi}(r_j)}{\partial x} &= -\delta_{ij}, & \frac{\partial N_{yi}(r_j)}{\partial y} &= 0.
\end{aligned}
\tag{9}
$$

Combining (4), (8) and (9), the partial derivatives of deflection function can be obtained:

$$
(\theta_x)_i = \left.\frac{\partial w}{\partial y}\right|_i = \frac{\partial N_i}{\partial y} w_i + \frac{\partial N_{xi}}{\partial y}\theta_{xi} + \frac{\partial N_{yi}}{\partial y}\theta_{yi} + N_i\,\theta_x^i = \theta_{xi} + \theta_x^i,
\tag{10}
$$

$$
(\theta_y)_i = -\left.\frac{\partial w}{\partial x}\right|_i = -\frac{\partial N_i}{\partial x} w_i - \frac{\partial N_{xi}}{\partial x}\theta_{xi} - \frac{\partial N_{yi}}{\partial x}\theta_{yi} + N_i\,\theta_y^i = \theta_{yi} + \theta_y^i.
\tag{11}
$$

According to (10) and (11), the global rotations $(\theta_x)_i$ and $(\theta_y)_i$ contained not only the local rotations θ_{xi} and θ_{yi}, but also the additional rotations θ_x^i and θ_y^i. The reason for this was that the partial derivatives of the first-order local deflection function were not equal to zero, and thus, additional terms appeared after differentiating the global deflection function, which corresponded to the additional rotations θ_x^i and θ_y^i. In

such a case, the relations between the global and local rotation functions in the zero-order approximation, shown in (12), did not hold anymore:

$$(\theta_x)_i = \theta_{xi}, \quad (\theta_y)_i = \theta_{yi}. \tag{12}$$

2.2. *Shape function.* In this study, the center of a rectangle served as the origin in the local coordinate system, and the ξ and η axes were parallel to the x and y axes, respectively, as shown in Figure 2. The transformation relations of these two coordinate systems can be expressed as

$$x = x_0 + a\xi, \quad y = y_0 + b\eta, \tag{13}$$

$$
\begin{aligned}
x_0 &= \tfrac{1}{2}(x_1 + x_3) = \tfrac{1}{2}(x_2 + x_4), \quad y_0 = \tfrac{1}{2}(y_1 + y_3) = \tfrac{1}{2}(y_2 + y_4), \\
a &= \tfrac{1}{2}(x_3 - x_1) = \tfrac{1}{2}(x_4 - x_2), \quad b = \tfrac{1}{2}(y_3 - y_1) = \tfrac{1}{2}(y_4 - y_2),
\end{aligned}
\tag{14}
$$

where (x_i, y_i) $(i = 1, 2, 3, 4)$ is the global coordinate of node i.

In the local coordinate system, the coordinate of node i is (ξ_i, η_i) $(i = 1, 2, 3, 4)$, and its value is ± 1. In this paper, the commonly used shape functions in the local coordinate $\xi_0\eta$ were adopted as

$$
\begin{aligned}
N_i &= \frac{(1 + \xi_0)(1 + \eta_0)(2 + \xi_0 + \eta_0 - \xi^2 - \eta^2)}{8}, \\
N_{xi} &= \frac{-b\eta_i(1 + \xi_0)(1 + \eta_0)(1 - \eta^2)}{8}, \quad (i = 1, 2, 3, 4), \\
N_{yi} &= \frac{a\xi_i(1 + \xi_0)(1 + \eta_0)(1 - \xi^2)}{8},
\end{aligned}
\tag{15}
$$

where $\xi_0 = \xi\xi_i$ and $\eta_0 = \eta\eta_i$. An element with the abovementioned shape functions can be easily proven to be a nonconforming element [Lascaux and Lesaint 1975; Reddy 2006].
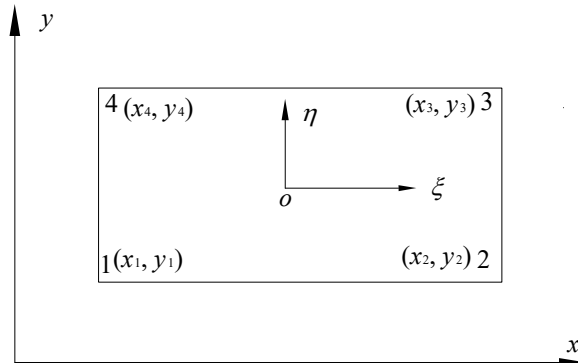
Figure 2. Global and local coordinate systems.

3. Element analyses

The total potential energy based on Kirchhoff's thin plate theory [Timoshenko and Woinowsky-Krieger 1959] can be expressed as

$$\Pi_p = \frac{1}{2} \iint_{\Omega} (\boldsymbol{\kappa}^T \boldsymbol{D} \boldsymbol{\kappa} - \bar{p} w) \, dx \, dy - \int_{S_3} \bar{q} w \, dS + \int_{S_M} \overline{M}_{\boldsymbol{n}} \frac{\partial w}{\partial \boldsymbol{n}} \, dS, \tag{16}$$

where $\boldsymbol{\Omega}$ indicates the solution domain, $\boldsymbol{\kappa}$ is the generalized strain, $\bar{p}$ is a distributed load, $\bar{q}$ is a linearly transverse load, $\overline{M}_n$ is a bending moment, and $\boldsymbol{n}$ is the exterior unit normal vector. A quantity under the bar "–" indicates that it is known, and $S_M = S_2 \cup S_3$.

In general, the boundary of $\boldsymbol{\Omega}$ can be divided into three disconnected parts, that is, $\partial \boldsymbol{\Omega} = S_1 \cup S_2 \cup S_3$ [Timoshenko and Woinowsky-Krieger 1959]. S_1 is clamped, if

$$\text{on } S_1: \quad w = \bar{w}, \quad \frac{\partial w}{\partial \boldsymbol{n}} = \bar{\varphi}_n, \tag{17}$$

where $\bar{w}$ is the deflection and $\bar{\varphi}_n$ is the normal angle. S_2 is simply supported, if

$$\text{on } S_2: \quad w = \bar{w}, \quad M_n = \overline{M}_n, \tag{18}$$

where $\overline{M}_n$ is the bending moment. S_3 is free, if

$$\text{on } S_3: \quad M_n = \overline{M}_n, \quad \frac{\partial M_{ns}}{\partial \boldsymbol{s}} + Q_n = \bar{q}, \tag{19}$$

where M_{ns} is the twisting moment, and Q_n is the lateral shear force.

The local frame on the boundary is constituted by $\boldsymbol{n}$ and $\boldsymbol{s}$ and displayed in Figure 3. The exterior unit normal vector $\boldsymbol{n}$ and the unit tangential vector $\boldsymbol{s}$ are defined as

$$\boldsymbol{n} = (n_x, n_y)^{\text{T}}, \quad \boldsymbol{s} = -(n_y, n_x)^{\text{T}}. \tag{20}$$

The transformations of the first-order derivatives can be written as

$$\frac{\partial}{\partial \boldsymbol{n}} = n_x \frac{\partial}{\partial x} + n_y \frac{\partial}{\partial y}, \quad \frac{\partial}{\partial \boldsymbol{s}} = -n_y \frac{\partial}{\partial x} + n_x \frac{\partial}{\partial y}. \tag{21}$$
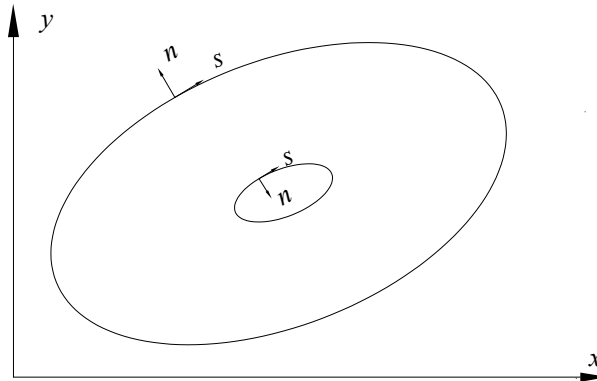

Figure 3. Definition of local frame.

The generalized strain $\boldsymbol{\kappa}$ can be expressed as

$$\{\boldsymbol{\kappa}\} = \left\{ \begin{array}{c} -\partial^2 w/\partial x^2 \\ -\partial^2 w/\partial y^2 \\ -2(\partial^2 w/\partial x\,\partial y) \end{array} \right\}, \tag{22}$$

$$\boldsymbol{D} = D \begin{bmatrix} 1 & \mu & 0 \\ \mu & 1 & 0 \\ 0 & 0 & 1-\mu \end{bmatrix}, \tag{23}$$

$$D = \frac{Eh^3}{12(1-\mu^2)}, \tag{24}$$

where D is the flexural rigidity of the plate, h is the thickness of a thin plate, E is the modulus of elasticity, and μ is the Poisson's ratio.

The FEM requires all of the nodes to be on the domain boundaries to impose the essential boundary conditions. This creates difficulties when dealing with complex boundaries, because considerable effort is required to solve the mismatch between the meshes and domain boundaries. Fortunately, by using the Lagrange multiplier method and penalty method, the essential boundary conditions can be weakly imposed in the NMM. In this paper, the essential boundary conditions were imposed by using the penalty method. The penalized formulation fitted to the total potential energy can be expressed as

$$\Pi_p^* = \Pi_p + \int_{S_w} \frac{1}{2} k_w (w - \overline{w})^2 \, dS + \int_{S_1} \frac{1}{2} k_M \left(\frac{\partial w}{\partial \boldsymbol{n}} - \bar{\varphi}_n \right)^2 dS, \tag{25}$$

where $S_w = S_1 \cup S_2$ is the essential boundary; k_w and k_M are the penalty parameters, and the suggested values are $10^3 E$–$10^5 E$.

4. Discretization scheme

According to the principle of minimum potential energy, letting $\delta \Pi_p^*(w) = 0$, the true deflection was obtained. The discretized algebraic equations can be written as

$$\boldsymbol{K}\boldsymbol{\delta} = \boldsymbol{f}, \tag{26}$$

where $\boldsymbol{K}$ is the global stiffness matrix, and $\boldsymbol{f}$ is the equivalent nodal force vector. Matrix $\boldsymbol{K}$ is obtained by assembling the stiffness matrix $\boldsymbol{K}^e$ from all of the elements and displacement boundary segments. Vector $\boldsymbol{f}$ is obtained by assembling the vector $\boldsymbol{f}^e$.

The nodal moment $\boldsymbol{M}$ can be derived as

$$\boldsymbol{M} = \boldsymbol{D}\boldsymbol{\kappa}, \tag{27}$$

where the generalized strain κ can be written as

$$\kappa = B\delta^e = \begin{bmatrix} B_1 & B_2 & B_3 & B_4 \end{bmatrix} \begin{bmatrix} \delta_1^\mathrm{T} & \delta_2^\mathrm{T} & \delta_3^\mathrm{T} & \delta_4^\mathrm{T} \end{bmatrix}^\mathrm{T},$$
$$B = \begin{bmatrix} B_1 & B_2 & B_3 & B_4 \end{bmatrix}, \quad \delta^e = \begin{bmatrix} \delta_1^\mathrm{T} & \delta_2^\mathrm{T} & \delta_3^\mathrm{T} & \delta_4^\mathrm{T} \end{bmatrix}^\mathrm{T}, \tag{28}$$

$$B_i = - \begin{bmatrix} \partial^2 N_i / \partial x^2 \\ \partial^2 N_i / \partial y^2 \\ 2(\partial^2 N_i / \partial x\, \partial y) \end{bmatrix} = - \begin{bmatrix} \frac{1}{a^2}(\partial^2 N_i / \partial \xi^2) \\ \frac{1}{b^2}(\partial^2 N_i / \partial \eta^2) \\ \frac{2}{ab}(\partial^2 N_i / \partial \xi\, \partial \eta) \end{bmatrix} = -\frac{1}{ab} \begin{bmatrix} \frac{b}{a}(\partial^2 N_i / \partial \xi^2) \\ \frac{a}{b}(\partial^2 N_i / \partial \eta^2) \\ 2(\partial^2 N_i / \partial \xi\, \partial \eta) \end{bmatrix}. \tag{29}$$

From (16), (25) and (26), the element stiffness matrix K^e is composed of the system stiffness matrix k, the matrices due to constrained deflection k_w, and normal rotation k_θ, as

$$K^e = k + k_w + k_\theta, \tag{30}$$

where the system stiffness matrix k can be divided into submatrices as

$$k = \begin{bmatrix} k_{11} & k_{12} & k_{13} & k_{14} \\ k_{21} & k_{22} & k_{23} & k_{24} \\ k_{31} & k_{32} & k_{33} & k_{34} \\ k_{41} & k_{42} & k_{43} & k_{44} \end{bmatrix}, \tag{31}$$

$$k_{ij} = \int_{\Omega_e} B_i^\mathrm{T} D B_j \, dx \, dy. \tag{32}$$

k_w and k_θ can be expressed as

$$k_w = \int_{S_w} k_w N^\mathrm{T} N \, dS, \quad k_\theta = \int_{S_1} k_M \frac{\partial N^\mathrm{T}}{\partial n} \frac{\partial N}{\partial n} dS. \tag{33}$$

The equivalent load vector can be expressed as

$$f^e = Q^e + \int_{S_w} \overline{w} k_w N^\mathrm{T} dS + \int_{S_w} \bar{\varphi}_n k_M \frac{\partial N^\mathrm{T}}{\partial n} dS, \tag{34}$$

$$Q^e = \begin{bmatrix} Q_1^\mathrm{T} & Q_2^\mathrm{T} & Q_3^\mathrm{T} & Q_4^\mathrm{T} \end{bmatrix}^\mathrm{T}. \tag{35}$$

Suppose that a thin plate is subjected to a bending moment $\overline{M}$, transverse line load $\bar{q}$, and uniformly distributed load of intensity $\bar{p}$, and thus, the equivalent nodal forces can be written as

$$Q_i = \begin{Bmatrix} F_{zi} \\ M_{\theta_{xi}} \\ M_{\theta_{yi}} \end{Bmatrix} = \iint_{\Omega_e} N_i^\mathrm{T} \bar{p} \, dx \, dy + \int_{S_3} N_i^\mathrm{T} \bar{q} \, ds - \int_{S_M} \frac{\partial N_i^\mathrm{T}}{\partial n} \overline{M} \, ds, \quad (i = 1, 2, 3, 4). \tag{36}$$

5. Numerical examples

5.1. *Rectangular plate with four edges simply supported subjected to distributed and concentrated loads.* A rectangular plate with four edges simply supported is shown in Figure 4. A distributed load of intensity q and a concentrated load p were exerted on the plate.
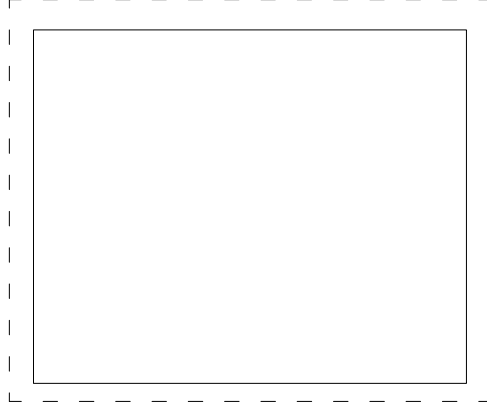
Figure 4. A rectangular plate with four edges simply supported.

The analytical solutions of the deflection in a simply supported plate subjected to a distributed load of intensity q [Reddy 2006] can be expressed as

$$w = \frac{16q}{\pi^6 D} \sum_{m=1,3,5,\ldots}^{\infty} \sum_{n=1,3,5,\ldots}^{\infty} \frac{\sin \frac{m\pi(x+a/2)}{a} \sin \frac{n\pi(y+b/2)}{a}}{mn(m^2/a^2 + n^2/b^2)^2}, \tag{37}$$

where $a = 1$ is the plate width, $b = 1$ is the plate length, $q = 1$, and $D = 1$.

The analytical solutions of the deflection in a simply supported plate subjected to a concentrated load p [Reddy 2006] can be expressed as

$$w = \frac{4p}{\pi^4 abD} \sum_{m=1,3,5,\ldots}^{\infty} \sum_{n=1,3,5,\ldots}^{\infty} (-1)^{(m+n)/2-1} \frac{\sin \frac{m\pi(x+a/2)}{a} \sin \frac{n\pi(y+b/2)}{a}}{(m^2/a^2 + n^2/b^2)^2}, \tag{38}$$

where $p = 1$.

The deflection error is defined as

$$w_{\mathrm{err}} = \frac{|\bar{w} - w|}{w} \times 100\%, \tag{39}$$

where w and $\bar{w}$ are the analytical and numerical solutions of the deflection, respectively. The meshes with 4×4, 8×8, 16×16, 32×32, 64×64 elements are displayed in Figure 5.
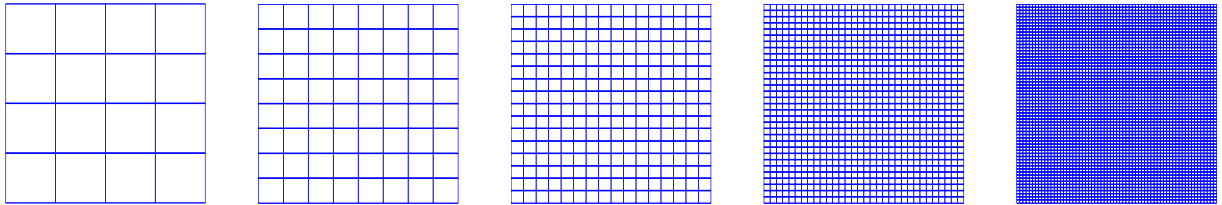
Figure 5. Calculational meshes with different elements of a simply supported rectangular plate; from left to right: 4×4, 8×8, 16×16, 32×32, 64×64.

Figures 6 and 7 show the deflection errors of a simply supported rectangular plate subjected to the distributed load and the concentrated load with the mesh with 64×64 elements achieved with the first-order NMM, respectively. The maximum deflection error of a simply supported rectangular plate subjected to the distributed load with the mesh with 64×64 elements, occurred at the four corners of the rectangular plate, was 0.046762%. The maximum deflection error subjected to the concentrated load, occurred at the center of the rectangular plate, was 0.050923%.

Figures 8 and 9 show the central deflections of a simply supported rectangular plate subjected to the distributed load and the concentrated load achieved with the FEM, the first-order NMM and the analytical method, respectively, and these results are listed in Table 1.

The results achieved with the first-order NMM compared well with the analytical solutions and were slightly better than those achieved with the FEM.
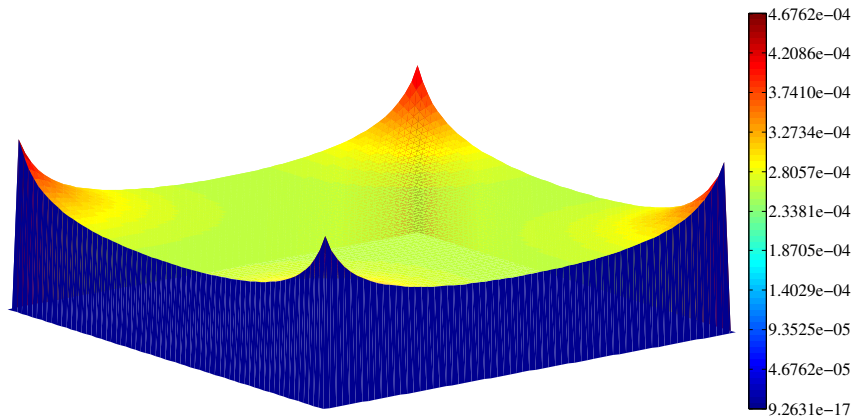
Figure 6. Deflection errors of a simply supported rectangular plate under distribute load using the first-order NMM with the mesh with 64×64 elements.
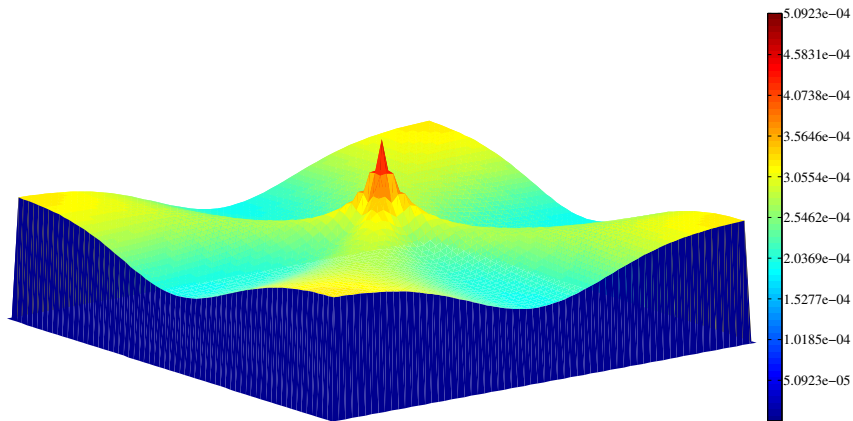
Figure 7. Deflection errors of a simply supported rectangular plate under concentrated load using the first-order NMM with the mesh with 64×64 elements.
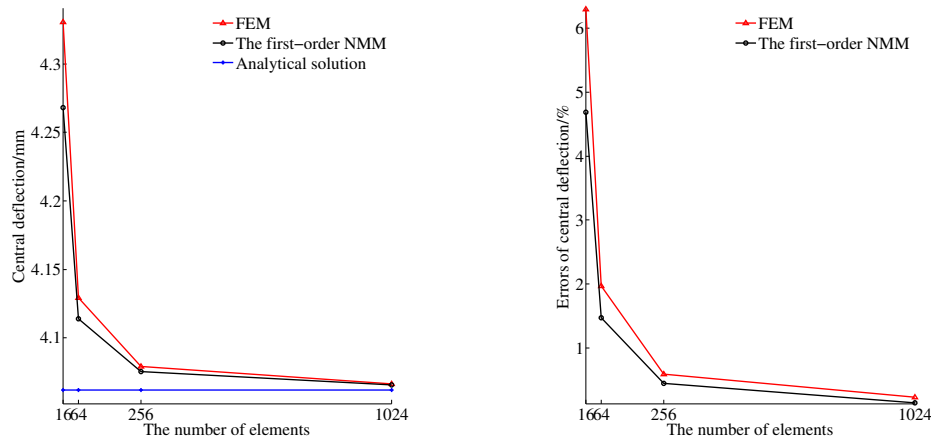
Figure 8. Central deflection comparisons of a simply supported rectangular plate under distributed load using the FEM, the first-order NMM and the analytical method.
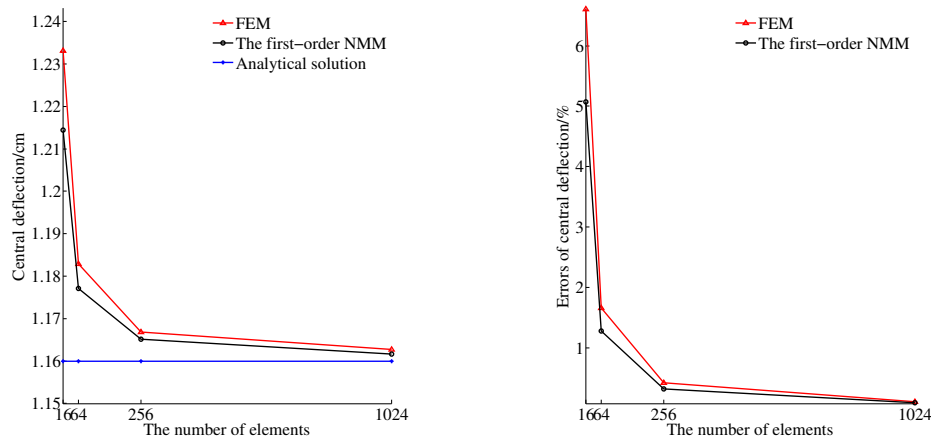
Figure 9. Central deflection comparisons of a simply supported rectangular plate under concentrated load using the FEM, the first-order NMM and the analytical method.

mesh size	distributed load (10^{-3} m)		concentrated load (10^{-2} m)	
	FEM	first-order NMM	FEM	first-order NMM
4×4	4.3304(6.61%)	4.2681(5.07%)	1.2331(6.30%)	1.2144(4.69%)
8×8	4.1293(1.66%)	4.1138(1.28%)	1.1829(1.97%)	1.1771(1.47%)
16×16	4.0791(0.42%)	4.0752(0.32%)	1.1669(0.59%)	1.1652(0.45%)
32×32	4.0665(0.11%)	4.0656(0.09%)	1.1627(0.23%)	1.1616(0.14%)
64×64	4.0634(0.03%)	4.0632(0.03%)	1.1607(0.06%)	1.1605(0.04%)
analytical solution	4.0620		1.1600	

Table 1. Central deflections of a simply supported rectangular plate under distributed and concentrated loads using the FEM, the first-order NMM and the analytical method.

5.2. *Clamped and simply supported circular plates subjected to distributed load.* Clamped and simply supported circular plates subjected to a distributed load of intensity q are shown in Figure 10.

The analytical solution of the deflection in a clamped circular plate subjected to a distributed load of intensity q [Reddy 2006] can be expressed as

$$w = \frac{q(x^2 + y^2 - r^2)}{64D}, \tag{40}$$

where $D = 1$, $q = 1$, and $r = 1$.

The analytical solution of the deflection in a simply supported circular plate subjected to a distributed load of intensity q [Reddy 2006] can be expressed as

$$w = \frac{q}{64D}\left[(x^2 + y^2 - r^2)^2 + \frac{4r^2(x^2 + y^2 - r^2)}{1 + \mu}\right], \tag{41}$$

where $\mu = 0.3$. The meshes used for the zero-order NMM and the first-order NMM are shown in Figure 11, and the meshes used for various FEM are shown in Figure 12.

To illustrate the efficiency of the first-order NMM developed in this study, the shell63-type element in ANSYS 10.0 developed by ANSYS Inc. (Pittsburgh, PA, USA), was selected to analyze this plate. The shell63-type element is a plate element with six parameters, the displacements in the directions of the x, y and z axes and the rotations about these three axes. Because the distributed load was perpendicular to the neutral surface, the displacements in the directions of the x and y axes and the rotation about the z axis were considered to be equal to zero. Thus, the shell63-type element can simulate the bending problems of thin plates.
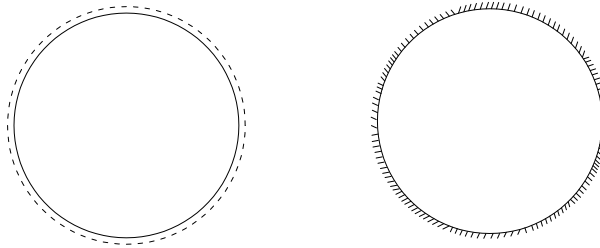
Figure 10. Circular plates: simply supported boundary (left) and clamped boundary (right).
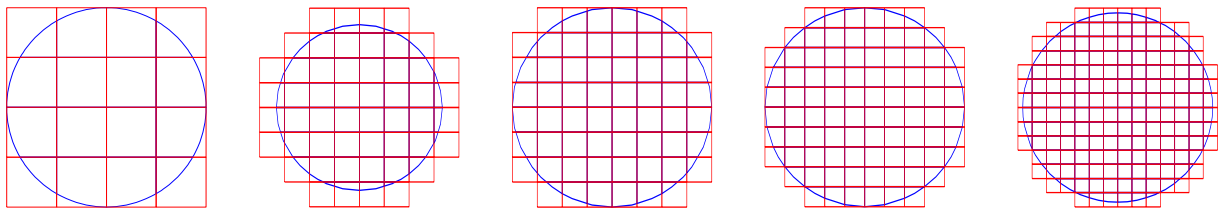
Figure 11. Calculational meshes with different element sizes of circular plates divided for the zero-order NMM and the first-order NMM; from left to right: 0.5×0.5, 0.3×0.3, 0.25×0.25, 0.2×0.2, 0.15×0.15.
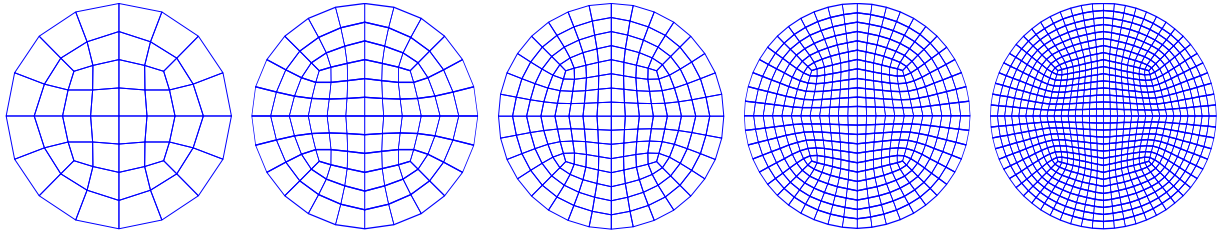
Figure 12. Calculational meshes with different elements of circular plates divided for various FEM; from left to right: 48, 108, 192, 432, 768.

Figures 13 and 14 show the deflections of clamped and simply supported circular plates subjected to a distributed load of intensity q achieved with the first-order NMM and the analytical method. The central deflections achieved with the zero-order NMM, the first-order NMM and the analytical method are listed in Table 2. The central deflections achieved with the shell63-type element in ANSYS 10.0, RPAQ [Cen et al. 2006; Long et al. 2005], TACQ [Cen and Long 1999] and the analytical method are listed in Table 3. In the first column of tables 2 and 3, the length represents the largest element diagonal. Figures 15 and 16 show the central deflections and their errors calculated with different methods.

The results achieved with the first-order NMM compared well with the analytical solutions and were much better than those calculated with the shell63-type element in ANSYS 10.0, RPAQ, TACQ and the zero-order NMM. The convergence processes of the central deflections of a clamped circular plate and a simply supported plate subjected to distributed load calculated with the zero-order NMM and the first-order NMM were oscillatory, and the trends of the deflection errors achieved with the two methods were similar.
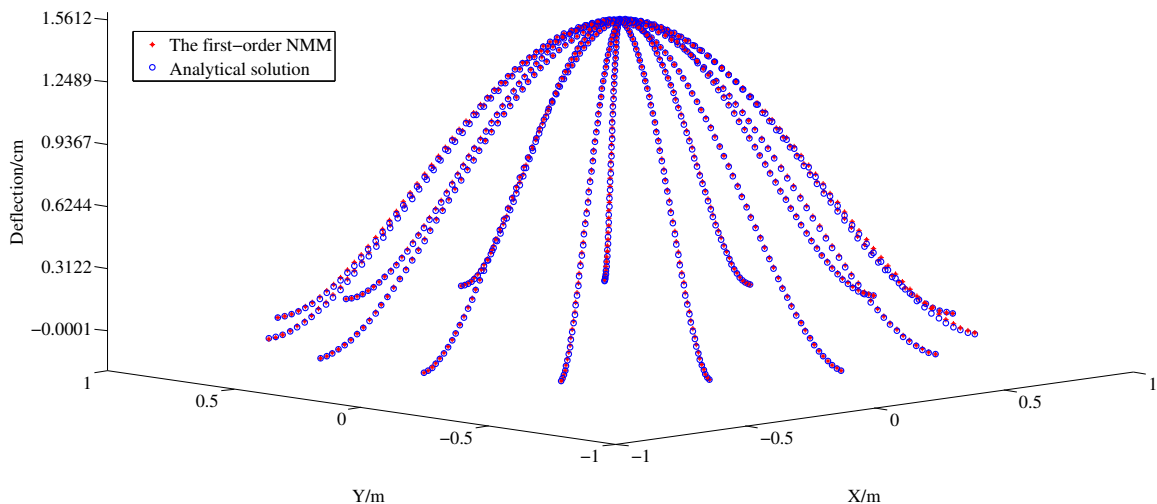
Figure 13. Deflection comparisons of a clamped circular plate under distributed load using the first-order NMM with 0.15×0.15 mesh and the analytical method.
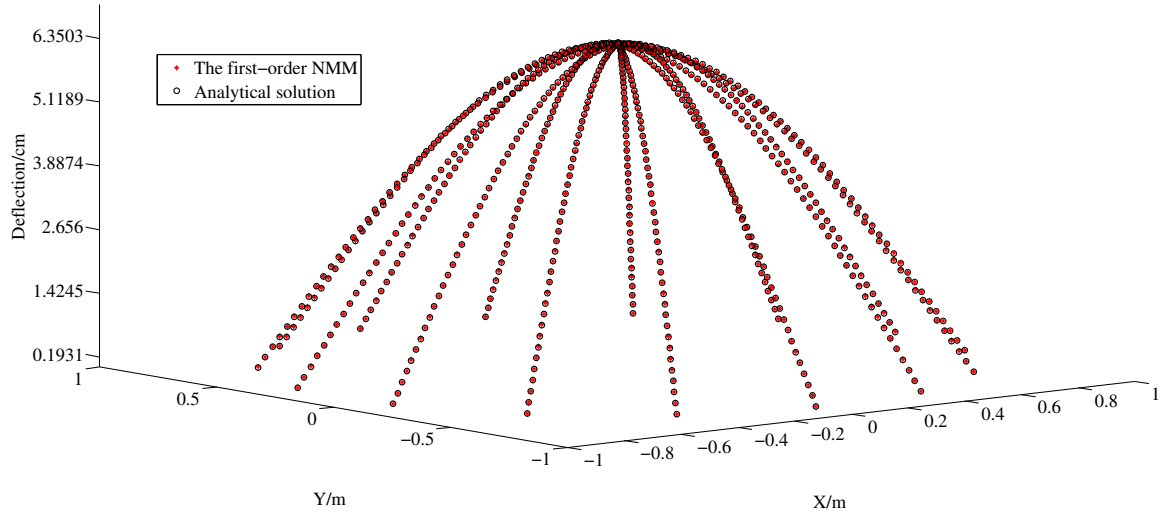
Figure 14. Deflection comparisons of a simply supported circular plate under distributed load using the first-order NMM with 0.15×0.15 mesh and the analytical method.

length (10^{-1} m)/	simply supported boundary (10^{-2} m)		clamped boundary (10^{-2} m)	
(element number)	zero-order NMM	first-order NMM	zero-order NMM	first-order NMM
7.0711/(16)	6.5251(2.43%)	6.5034(2.09%)	1.6466(5.38%)	1.5997(2.38%)
4.2426/(52)	6.3512(0.3%)	6.3561(0.22%)	1.5717(0.59%)	1.5463(1.04%)
3.5355/(60)	6.3569(0.21%)	6.3813(0.17%)	1.5629(0.03%)	1.5586(0.25%)
2.8284/(88)	6.3813(0.17%)	6.3747(0.07%)	1.5553(0.46%)	1.5629(0.03%)
2.1213/(164)	6.3535(0.26%)	6.3741(0.06%)	1.5628(0.02%)	1.5622(0.02%)
analytical solution	6.3702		1.5625	

Table 2. Central deflections of simply supported and clamped circular plates under distributed load using the zero-order NMM, the first-order NMM and the analytical method.

length (10^{-1} m)/	simply supported boundary (10^{-2} m)			clamped boundary (10^{-2} m)		
(element number)	FEM	RPAQ	TACQ	FEM	RPAQ	TACQ
7.368/(48)	6.2753(1.49%)	6.541(2.68%)	–	1.5819(1.24%)	1.264(19.1%)	–
4.3051/(108)	6.3285(0.65%)	6.414(0.69%)	6.4088(0.61%)	1.5715(0.58%)	1.484(5.02%)	1.4790(5.34%)
2.3301/(192)	6.3469(0.37%)	6.381(0.17%)	6.3807(0.16%)	1.5672(0.3%)	1.543(1.25%)	1.5422(1.30%)
1.5696/(432)	6.3599(0.16%)	–	–	1.5644(0.12%)	–	–
1.1814/(768)	6.3644(0.09%)	–	–	1.5635(0.06%)	–	–
analytical solution	6.3702			1.5625		

Table 3. Central deflections of simply supported and clamped circular plates under distributed load using the FEM, RPAQ [Cen et al. 2006], TACQ [Cen and Long 1999] and the analytical method.
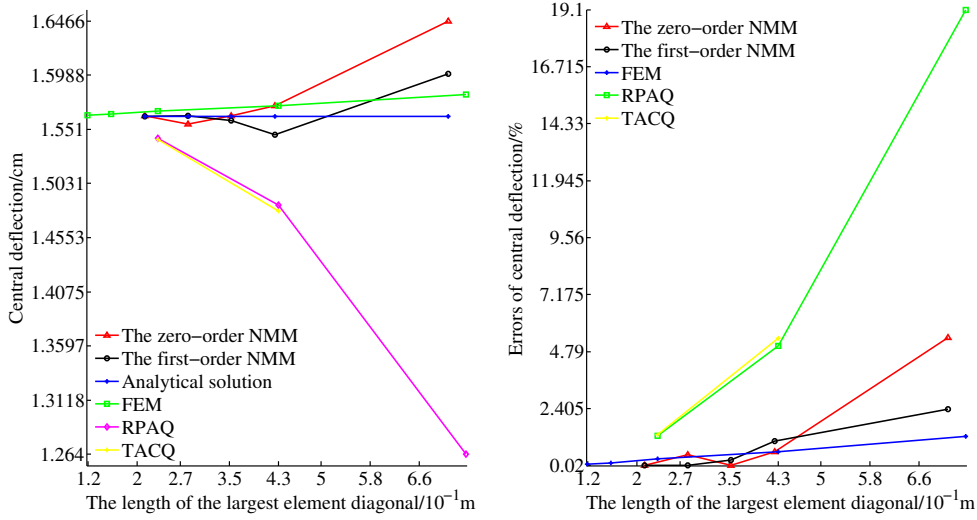
Figure 15. Central deflections and error comparisons of a clamped circular plate under distributed load using the different methods.
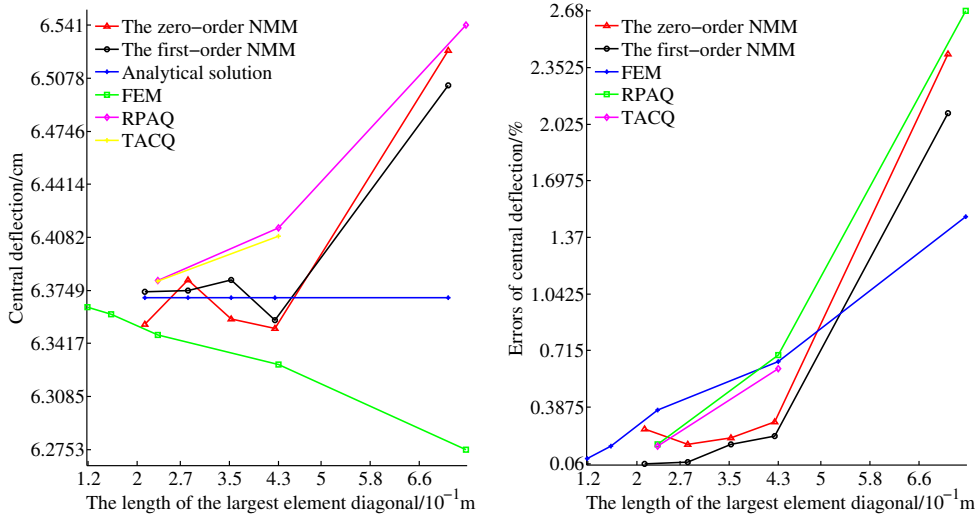
Figure 16. Central deflections and error comparisons of a simply supported circular plate under distributed load using different methods.

5.3. *Simply supported annular plate subjected to transverse line load.* An annular plate depicted in Figure 17 (left) with the inner edge subjected to a transverse line load p was studied here, with its outer edge simply supported and its inner edge free. The analytical solution of the deflection for this numerical example [Reddy 2006] can be expressed as

$$w = \frac{pba^2}{8D}\left[\left(1 - \frac{x^2+y^2}{a^2}\right)\left(\frac{3+\mu}{1+\mu} - 2\kappa\right) + \frac{2(x^2+y^2)}{a^2}\ln\sqrt{\frac{x^2+y^2}{a^2}} + 4\kappa\left(\frac{1+\mu}{1-\mu}\right)\ln\sqrt{\frac{x^2+y^2}{a^2}}\right], \quad (42)$$

where $\kappa = \beta^2/(1 - \beta^2) \ln \beta$, $\beta = b/a$, $p = 0.01$, $\mu = 0.3$, with $a = 5$ and $b = 1$ as the outer and inner radii of the annular plate, respectively. The mesh used for the zero-order NMM and the first-order NMM is shown in Figure 17 (middle), and the mesh with 3200 elements used for the FEM is shown in Figure 17 (right).

Figure 18 displays the deflections and deflection errors of a simply supported annular plate with the inner edge subjected to transverse line load achieved with the first-order NMM. The maximum deflection error that occurred at the inner edge was 3.8637%. Figure 19 shows the numerical solutions of the deflection on the line $y = 0$ and the corresponding analytical solutions achieved with the first-order NMM, the zero-order NMM, the FEM and the analytical method. The deflections achieved with the first-order NMM compared well with the analytical solutions and were much better than those achieved with the zero-order NMM and the FEM.

Compared with the above methods discussed in the examples, the results calculated with the first-order NMM introduced in this study were more accurate than those achieved with the other methods, since the first-order NMM incorporated both the regular meshes and the first-order displacement function in the bending analysis of nonconforming thin plates. Additionally, the validity of the first-order NMM was verified by comparing the results of the above three examples.
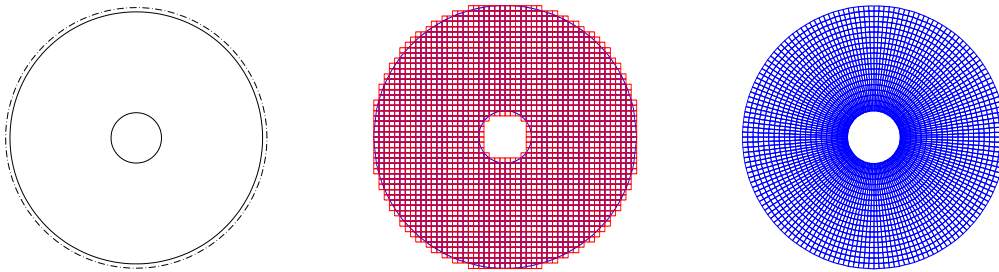
Figure 17. An annular plate: simply supported boundary (left); 0.2×0.2 mesh divided for the first-order NMM and the zero-order NMM (middle); the mesh with 3200 elements divided for the FEM (right).
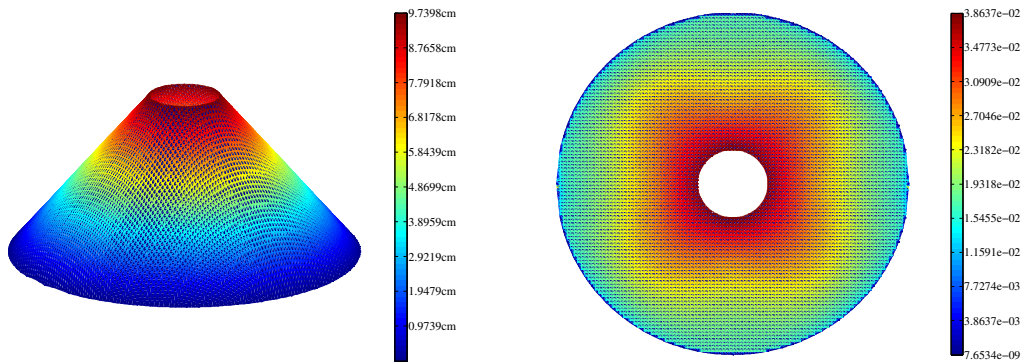
Figure 18. Results of a simply supported annular plate subjected to transverse line load using the first-order NMM with 0.2×0.2 mesh: deflections (left) and deflection errors (right).
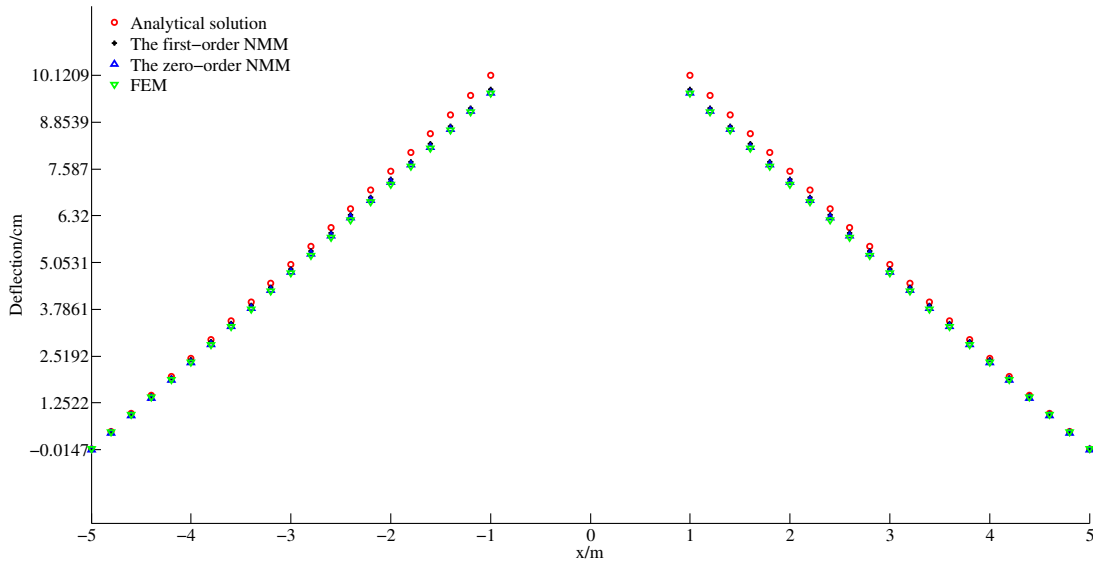
Figure 19. Deflection comparisons of a simply supported annular plate subjected to transverse line load using the different methods.

6. Conclusions

The major advantage of the NMM over the FEM is that it adopts two completely independent covers, which allows the best meshes to be selected as the mathematical cover for interpolation to improve the convergence performance. Another feature is the flexibility in constructing the local displacement function. Using these properties, the first-order NMM was developed to solve the convergence issues of nonconforming elements and improve the accuracy and efficiency. Compared with other methods of upgrading the order of the approximation function, the first-order Taylor expansion endows the generalized degrees of freedom with physical meanings and decreases the rank deficiency. Additionally, the first-order approximation is the most economical way to upgrade the order of the local deflection function. Importantly, the new relations between the global and local rotation functions in the first-order approximation were derived by adopting two sets of rotation functions, $\{\theta_{xi}, \theta_{yi}\}$ and $\{\theta_x{}^i, \theta_y{}^i\}$. The discussed examples showed that the numerical solutions achieved with the first-order NMM rapidly converged to the analytical solutions and their accuracy was vastly superior to that achieved with the FEM and the zero-order NMM, which verified the first-order NMM.

References

[Bazeley et al. 1965] G. P. Bazeley, Y. K. Cheung, B. M. Irons, and O. C. Zienkiewicz, "Triangular elements in plate bending — conforming and non-conforming solutions", pp. 547–576 in *Proceedings of the 1st Conference on Matrix Methods in Structural Mechanics* (Dayton), 1965.

[Cen and Long 1999] S. Cen and Y. Q. Long, "A quadrilateral thin-thick plate bending element by using area coordinate method", *Eng. Mech.* **16**:2 (1999), 1–15.

[Cen et al. 2006] S. Cen, Y. Q. Long, Z. H. Yao, and S. P. Chiew, "Application of the quadrilateral area co-ordinate method: a new element for Mindlin–Reissner plate", *Int. J. Numer. Methods Eng.* **66**:1 (2006), 1–45.

[Ciarlet 1978] P. G. Ciarlet, *The finite element method for elliptic problems*, North-Holland, Amsterdam, 1978.

[Deng and Murakawa 2008] D. Deng and H. Murakawa, "Prediction of welding distortion and residual stress in a thin plate butt-welded joint", *Comput. Mater. Sci.* **43**:2 (2008), 353–365.

[Kersemans et al. 2014] M. Kersemans, A. Martens, N. Lammens, K. Van Den Abeele, J. Degrieck, F. Zastavnik, L. Pyl, H. Sol, and W. Van Paepegem, "Identification of the elastic properties of isotropic and orthotropic thin-plate materials with the pulsed ultrasonic polar scan", *Exp. Mech.* **54**:6 (2014), 1121–1132.

[Lascaux and Lesaint 1975] P. Lascaux and P. Lesaint, "Some nonconforming finite elements for the plate bending problem", *R.A.I.R.O. Analyse Numérique* **9**:R1 (1975), 9–53.

[Liu and Trung 2010] G. R. Liu and N. T. Trung, *Smoothed finite element methods*, CRC Press, Boca Raton, 2010.

[Long et al. 2005] Y. Q. Long, X. M. Chen, and S. Cen, "A locking-free and robust quadrilateral reissner plate element", *Chin. J. Comput. Mech.* **22**:4 (2005), 385–391.

[Luo et al. 2010] S. M. Luo, W. B. Wen, S. Y. Chen, and Z. R. Zhang, "A new triangular element of numerical manifold method", *J. Plast. Eng.* **17**:6 (2010), 131–135.

[Miyazaki et al. 2016] H. Miyazaki, Y. Yoshizawa, K. Hirao, T. Ohji, and H. Hyuga, "Round-robin test on the fracture toughness of ceramic thin plates through modified single edge-precracked plate method", *J. Eur. Ceram. Soc.* **36**:13 (2016), 3245–3248.

[Qu and Zheng 2014] X. Qu and H. Zheng, "Mixed-order manifold method based on Taylor expansion", *J. Yangtze Riv. Scienti. Res. Ins.* **31**:8 (2014), 87–92.

[Qu et al. 2016] X. Qu, H. Zheng, L. J. Su, and C. G. Li, "Incompatible manifold method for thin plate problems based on the best quality mesh", *Chin. J. Comput. Mech.* **33**:6 (2016), 819–825.

[Reddy 2006] J. N. Reddy, *Theory and analysis of elastic plates and shells*, CRC Press, Boca Raton, 2006.

[Shi 1984] Z. C. Shi, "The generalized patch test for zienkiewicz's triangles", *J. Comput. Math.* **2**:3 (1984), 279–286.

[Shi 1990] Z. C. Shi, "On the accuracy of the quasi-conforming and generalized conforming finite elements", *Chin. Ann. Math. Ser. B* **11**:2 (1990), 148–155.

[Shi 1991] G. H. Shi, "Manifold method of material analysis", pp. 57–76 in *Transactions of the Ninth Army conference on applied mathematics and computing* (Minneapolis), 1991.

[Tang et al. 1981] L. M. Tang, W. J. Chen, and Y. X. Liu, "The quasi-conforming elements for thin plate bending analysis", *J. Build. Struct.* **2** (1981), 10–22.

[Timoshenko and Woinowsky-Krieger 1959] S. Timoshenko and S. Woinowsky-Krieger, *Theory of plates and shells*, 2nd ed., McGraw-Hill Book Company, 1959.

[Wang 2003] X. C. Wang, *The finite element methods*, Tsinghua University Press, Beijing, 2003.

[Wen and Luo 2012] W. B. Wen and S. M. Luo, "Polygonal manifold element for thin plate bending analysis", *Eng. Mech.* **29**:10 (2012), 249–256.

[Xie 2009] P. L. Xie, *Nonconforming finite element methods for the fourth order elliptic problems*, Fudan University, Shanghai, 2009.

[Xing and Liu 2009] Y. F. Xing and B. Liu, "High-accuracy differential quadrature finite element method and its application to free vibrations of thin plate with curvilinear domain", *Int. J. Numer. Methods Eng.* **80**:13 (2009), 1718–1742.

[Xu et al. 2014] D. D. Xu, H. Zheng, and Y. T. Yang, "Linearly independent higher-order numerical manifold method", *Chin. J. Geotech. Eng.* **36**:3 (2014), 482–488.

[Zhang et al. 2010] Z. R. Zhang, X. W. Zhang, and W. G. Lü, "numerical method based on compatible manifold element for thin plate bending", *Chin. J. Mech. Eng.* **23**:1 (2010), 100–109.

[Zhao 1988] J. Q. Zhao, "Discussion on constructing principle and convergence problem of the generalized conforming element", *J. Civil Eng.* **21**:4 (1988), 35–37.

[Zheng et al. 2013] H. Zheng, Z. J. Liu, and X. R. Ge, "Numerical manifold space of Hermitian form and application to Kirchhoff's thin plate problems", *Int. J. Numer. Methods Eng.* **95**:9 (2013), 721–739.

[Zhou and Deng 2008] X. Y. Zhou and A. F. Deng, "Numerical manifold method of analysis for beam and plate based ongeneralized variational principle", *Chin. J. Solid Mech.* **29**:3 (2008), 313–318.

[Zienkiewicz and Taylor 2005] O. C. Zienkiewicz and R. L. Taylor, *The finite element method for solid and structural mechanics*, 6th ed., Butterworth-Heinemann, 2005.

XIN QU: xqu1987@163.com
School of Civil and Architecture Engineering, Anyang Institute of Technology, Anyang 455000, China

FANGFANG DIAO: diaoff1986@163.com
School of Foreign Languages, Anyang Institute of Technology, Anyang 455000, China

XINGQIAN XU: xuxingqian_123@163.com
College of Water Conservancy, Yunnan Agricultural University, Kunming 650201, China

WEI LI: liw9012@163.com
Institute of Civil Engineering and Architecture, Linyi University, Linyi 276005, China

JOURNAL OF MECHANICS OF MATERIALS AND STRUCTURES

msp.org/jomms

Founded by Charles R. Steele and Marie-Louise Steele